Journal of Mathematical Biology (2024) 88:39
https://doi.org/10.1007/s00285-024-02061-4

Mathematical Biology

The influence of synaptic plasticity on critical coupling estimates for neural populations

Kaitlyn Toth[1] · Dan Wilson[1]

Received: 25 May 2023 / Revised: 31 January 2024 / Accepted: 4 February 2024 /
Published online: 5 March 2024

Abstract

The presence or absence of synaptic plasticity can dramatically influence the collective behavior of populations of coupled neurons. In this work, we consider spike-timing dependent plasticity (STDP) and its resulting influence on phase cohesion in computational models of heterogeneous populations of conductance-based neurons. STDP allows for the influence of individual synapses to change over time, strengthening or weakening depending on the relative timing of the relevant action potentials. Using phase reduction techniques, we derive an upper bound on the critical coupling strength required to retain phase cohesion for a network of synaptically coupled, heterogeneous neurons with STDP. We find that including STDP can significantly alter phase cohesion as compared to a network with static synaptic connections. Analytical results are validated numerically. Our analysis highlights the importance of the relative ordering of action potentials emitted in a population of tonically firing neurons and demonstrates that order switching can degrade the synchronizing influence of coupling when STDP is considered.

Keywords Synchronization · Neuroscience · Phase models · Synaptic plasticity · Phase cohesion · Critical coupling strength · Oscillations

Mathematics Subject Classification 37N25 · 92B25 · 34C15

1 Introduction

Neural synchrony is thought to play a key role in cognitive processing (Hipp et al. 2011; Senkowski et al. 2008), is a hallmark of the neural dysfunction that manifests

✉ Dan Wilson
dwilso81@utk.edu

[1] Department of Electrical Engineering and Computer Science, University of Tennessee, Knoxville, TN 37966, USA

in Parkinson's disease (Pogosyan et al. 2010; Wichmann et al. 2011), and is essential in the maintenance of circadian rhythms (Golombek and Rosenstein 2010; Reppert and Weaver 2002). Synchronization among large populations of coupled neurons has been widely studied from a dynamical systems perspective, yielding insight into the mechanisms by which neural synchronization emerges in conductance-based models of tonically firing neurons (Brown et al. 2003; Ermentrout 1996; Ermentrout and Terman 2010; Hansel et al. 1995; Hoppensteadt and Izhikevich 1997; Van Vreeswijk et al. 1994), and providing insight into strategies by which pathological synchronization can be suppressed (Holt et al. 2016; Pyragas et al. 2018; Toth and Wilson 2022; Wilson 2020). The vast majority of the phase-based analysis of neural oscillators, however, neglects the influence of synaptic plasticity. Often summarized by the aphorism: 'neurons that fire together, wire together', synaptic plasticity refers to the widely observed characteristic of real neurons to modify the strength of synaptic connections over time in response to the relative firing time between neurons (Ho et al. 2011; Kennedy 2013; Khoshkhou and Montakhab 2019). Recent evidence suggests synaptic plasticity is critical to the brain's ability to learn from memory (Kennedy 2013) motivating its implementation in artificial spiking neural networks to develop machine learning algorithms capable of pattern, image, and feature recognition (Iakymchuk et al. 2015; Manna et al. 2022).

Incorporation of spike-timing dependent plasticity (STDP) in computational models of synaptically coupled populations of neurons can have profound effects on their collective behavior. This point is illustrated by numerical simulations summarized in Figs. 1 and 2 for a population of $N = 5$ homogeneous neurons of the form

$$C\dot{V}_i = -I^i_{ion} - \frac{1}{N-1}\sum_{j\neq i} I^{j\to i}_{syn}, \tag{1}$$

for $i = 1, \ldots, N$, where V_i is the neural membrane potential (in mV), I^i_{ion} represents the ionic current derived from the neuron's internal dynamics, $I^{j\to i}_{syn}$ represents the synaptic current from the presynaptic neuron j to the postsynaptic neuron i, and C is the constant membrane capacitance. Since self coupling is not considered here, the $I^{j\to i}_{syn}$ term is scaled by $1/(N-1)$ and not $1/N$. The synaptic current is (Ermentrout and Terman 2010)

$$I^{j\to i}_{syn} = K g_{j\to i}(t) s_j(t)(V_i - E_{syn}), \tag{2}$$

where $K > 0$ is a maximum synaptic conductance, $g_{j\to i} \in [g_{min}, 1]$ is governed by a Hebbian STDP rule where the update is a function of the current weight of the synaptic connection and the time difference between spikes (Van Rossum et al. 2012), s_j is a synaptic variable associated with neuron j, and E_{syn} is the reversal potential that governs whether coupling is inhibitory or excitatory. A complete description of the model parameters can be found in Sect. 2. Figures 1 and 2 present the voltage dynamics and the corresponding Kuramoto order parameter using inhibitory and excitatory coupling, respectively. The Kuramoto order parameter, ζ, is used to quantify the level of synchronization with $\zeta = 1$ indicating complete synchronization and lower values indicating less synchronization in the network (the full definition of the

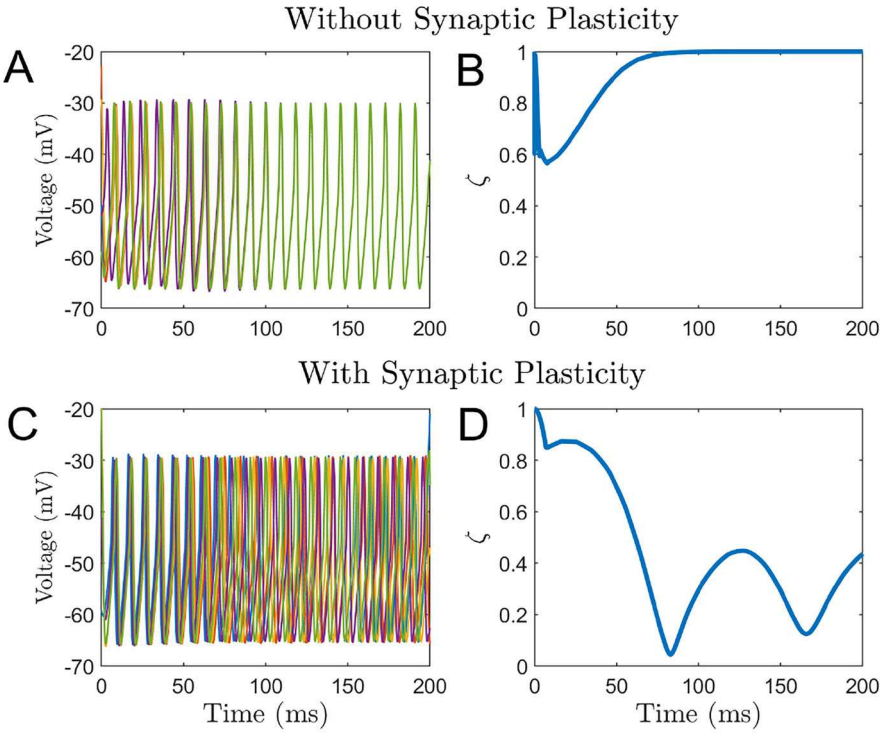

Fig. 1 Representative simulations for an inhibitory neural population with and without synaptic plasticity. Panel **A** shows the voltage dynamics of a homogeneous population of five neurons with inhibitory coupling and a static synaptic coupling strength of $Kg_{j\to i} = 0.1\,\mathrm{mS/cm^2}$ for all i and j. Panel **B** shows the corresponding Kuramoto order parameter indicating stable synchronization. Panel **C** shows the voltage dynamics of the same network with Hebbian STDP where $g_{j\to i} \in [0, 1]$ is allowed to change in time as described in Sect. 2.2. Panel **D** shows the associated Kuramoto order parameter

order parameter for this network is given in Eq. (10)). In both figures, panels A and B show the results with static coupling. Panels C and D in each figure provide the same information when using a Hebbian STDP rule instead. In both simulations, stability of the synchronous state depends on the presence or absence of synaptic plasticity in the network leading to substantial changes in the aggregate behavior. Figures 1 and 2 demonstrate that the presence or absence of synaptic plasticity can have a substantial influence on the aggregate behavior of a coupled population of neurons. Figure 1 demonstrates that a population of inhibitory neurons with static synaptic coupling and dynamics governed by (1) and (2) will tend toward a stable synchronized state. However, the inclusion of STDP prohibits this same population from synchronizing. Figure 2 illustrates that a homogenous population of excitatory neurons with static synaptic coupling and dynamics governed by (1) and (2) will tend toward a stable antiphase state. However, the inclusion of STDP allows this same population to reach a phase cohesive state.

While the dynamics that govern synaptic plasticity are well documented (Dayan and Abbott 2001) and often included in computational studies, its influence on network

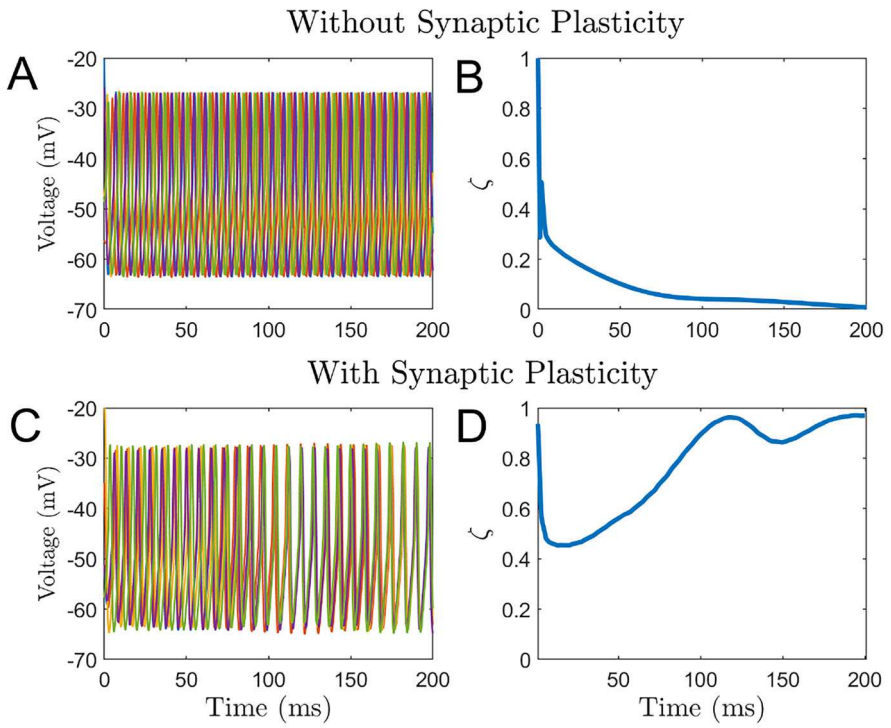

Fig. 2 Representative simulations for an excitatory neural population with and without synaptic plasticity. Panel **A** shows the voltage dynamics of a homogeneous population of five neurons with excitatory coupling and a static synaptic coupling strength of $Kg_{j\to i} = 0.1\,\mathrm{mS/cm^2}$ for all i and j. Panel **B** shows the associated Kuramoto order parameter indicating near complete desynchronization. Panel **C** shows the voltage dynamics of the same network with Hebbian STDP where $g_{j\to i} \in [0, 1]$ is allowed to change in time as described in Sect. 2.2 and Panel **D** gives the corresponding Kuramoto order parameter

synchronization is of particular interest in this work. Reference (Nowotny et al. 2003) concludes that STDP enhances neural synchronization when compared to populations of neurons without plastic synaptic coupling in results obtained on a hybrid network comprised of a spike generator, a clamp to simulate an excitatory synapse, and a neuron from an *Aplysia* abdominal ganglion. Reference (Karbowski and Ermentrout 2002) analyzes the parameters and factors that contribute to the development of a stable synchronized state in a population of heterogeneous excitatory oscillators coupled with STDP. Reference (Levy et al. 2001) studies the emergence of distributed synchrony throughout a population of coupled neurons with STDP. Reference (Maistrenko et al. 2007) discusses bifurcations in stability that occur among populations of Kuramoto oscillators coupled with STDP as the synaptic potentiation and depression windows change, with a stable synchronous state existing above some threshold coupling strength for equal window lengths and the emergence of multistability with asymmetric windows. Reference (Ozkan et al. 2014) analyzes how various parameters affect both the induction and retention of phase and period locking in a two-neuron network with plastic synaptic connections, and reference (Khoshkhou and Montakhab

2019) focuses on the effect of the axonal delay in a network of conductance-based neural oscillators with plastic synaptic connections in the context of the critical brain hypothesis (Chialvo 2010; Levina et al. 2007). In this work, we are primarily focused on understanding the synchronization (or lack thereof) that emerges in large populations of neurons with synaptic connections that are subject to Hebbian STDP rules as illustrated, for instance, in Figs. 1 and 2. While much research has been conducted on the implications of STDP on synchronization, none has addressed the existence of a threshold critical coupling strength for phase cohesion and the conditions which would affect this critical coupling strength. This work extends prior work from Wilson et al. (2018) to investigate the impact of Hebbian STDP on the critical coupling strength required to maintain phase cohesion.

Extending prior results from Wilson et al. (2018) that did not consider STDP, we derive upper bounds for the critical coupling strength required to maintain phase cohesion in a network of neurons with excitatory coupling and STDP. Note here that the critical coupling strength is the minimum coupling strength required to retain phase cohesion. Here, a population of oscillators is considered phase cohesive if the phase difference between any two oscillators remains bounded within a prespecified arclength. Critically, we find that the presence or absence of STDP can lead to qualitatively different collective behavior of the aggregate population. Our analysis highlights the importance of the relative ordering between phase cohesive neurons and that order switching can degrade the synchronizing influence of coupling when STDP is considered. The organization of this paper is as follows: in Sect. 2 we provide necessary background on the neural models used in this study in addition to the phase reduction techniques used to represent the oscillatory dynamics with a low order basis. In Sect. 3 we derive upper bounds on the critical coupling strength to maintain phase cohesion. Section 4 shows the result of numerical simulations validating our analytical results, and Sect. 5 provides concluding remarks.

2 Background

2.1 Neural model equations

The theoretical analysis presented in this work can be applied to any tonically firing conductance-based neural model. For concreteness, and for the purposes of illustration, we will consider a synaptically coupled model of a population of thalamic neurons from Rubin and Terman (2004)

$$\begin{aligned} C\dot{V}_i &= -I_L(V_i) - I_{Na}(V_i, h_i) - I_K(V_i, h_i) - I_T(V_i, r_i) + I_{stim,i} - \frac{1}{N-1}\sum_{j\neq i} I_{syn}^{j\to i}(s_j, V_i), \\ \dot{h_i} &= (h_\infty - h_i)/\tau_h, \\ \dot{r_i} &= (r_\infty - r_i)/\tau_r, \\ \dot{s_i} &= \frac{c_1(1-s_i)}{1+\exp(-(V_i - V_T)/\sigma_T)} - c_2 s_i, \end{aligned} \tag{3}$$

for $i = 1, \ldots, N$. Above, V_i denotes the transmembrane voltage of neuron i, h_i and r_i are associated gating variables, s_i is a state variable used to determine the synaptic current, and $C = 1\,\mu\text{F/cm}^2$ is the constant membrane capacitance. The synaptic current $I_{syn}^{j\to i}$, was defined in Eq. (2). Parameters that govern the dynamics of the synaptic variable are $c_1 = 3\ \text{ms}^{-1}$, $c_2 = 0.3\ \text{ms}^{-1}$, $V_T = -20$ mV, and $\sigma_T = 0.8$ mV. The form of Hebbian plasticity implemented in this model is discussed in the next subsection. I_L, I_{Na}, I_K, and I_T are the leak, sodium, potassium, and low-threshold calcium ionic currents, respectively, with dynamics

$$\begin{aligned} I_L(V) &= g_L(V - E_L), \\ I_{Na}(V,h) &= g_{Na}(m_\infty^3)h(V - E_{Na}), \\ I_K(V,h) &= g_K((0.75(1-h))^4)(V - E_K), \\ I_T(V,r) &= g_T(p_\infty^2)r(V - E_T), \end{aligned} \tag{4}$$

where $g_L = 0.05\ \text{mS/cm}^2$, $g_{Na} = 3\ \text{mS/cm}^2$, $g_K = 5\ \text{mS/cm}^2$, $g_T = 5\ \text{mS/cm}^2$, $E_L = -70$ mV, $E_{Na} = 50$ mV, $E_K = -90$ mV, and $E_T = 0$ mV. $I_{stim,i} \in [4.84, 5.16]$ is a baseline current applied to neuron i chosen so that the individual neurons are in a tonically firing regime. For homogeneous cases, $I_{stim,i} = 5$ for all N neurons. However, we will ultimately be looking specifically at situations where $I_{stim,i}$ is different between neurons yielding a heterogeneous population. Auxiliary functions are given below:

$$\begin{aligned} h_\infty &= 1/(1 + \exp((V + 41)/4)), \\ r_\infty &= 1/(1 + \exp((V + 84)/4)), \\ \alpha_h &= 0.128\exp(-(V + 46)/18), \\ \beta_h &= 4/(1 + \exp(-(V + 23)/5)), \\ \tau_h &= 1/(\alpha_h + \beta_h), \\ \tau_r &= 28 + \exp(-(V + 25)/10.5), \\ m_\infty &= 1/(1 + \exp(-(V + 37)/7)), \\ p_\infty &= 1/(1 + \exp(-(V + 60)/6.2)). \end{aligned} \tag{5}$$

2.2 Modelling synaptic plasticity

To incorporate synaptic plasticity, we consider a soft bound spike-timing dependent plasticity (STDP) rule (Khoshkhou and Montakhab 2019). In the context of Eq. (2), the STDP is incorporated by updating $g_{j\to i}(t) \in [g_{min}, 1]$ each time either neuron i or j spike. We specifically register an action potential or spike time whenever $V_i = -30$ mV and $\dot{V}_i > 0$. For two arbitrary neurons i and j, letting t_i be the time that neuron i spikes and t_j be the time that neuron j most recently spikes, immediately after neuron i spikes, both $g_{j\to i}(t)$ and $g_{i\to j}(t)$ are updated according to

$$g_{\alpha\to\beta}(t_i^+) = \begin{cases} g_{\alpha\to\beta}(t_i^-) + A_+(1 - g_{\alpha\to\beta}(t_i^-))e^{\frac{-\Delta t_{\alpha\to\beta}}{\tau_+}}, & 0 < \Delta t_{\alpha\to\beta} < t_c, \\ g_{\alpha\to\beta}(t_i^-) - A_-(g_{\alpha\to\beta}(t_i^-) - g_{min})e^{\frac{\Delta t_{\alpha\to\beta}}{\tau_-}}, & -t_c < \Delta t_{\alpha\to\beta} \leq 0, \\ g_{\alpha\to\beta}(t_i^-), & |\Delta t_{\alpha\to\beta}| \geq t_c, \end{cases} \tag{6}$$

where $\alpha = \{i, j\}$, $\beta = \{j, i\}$, and $\Delta t_{\alpha\to\beta} = t_\beta - t_\alpha$. Above, g_{min} is a lower bound on the synaptic strength (typically at or near 0). The magnitude of each update is determined by the amplitudes $A_+ = A_- = 2$, and the size of the synaptic potentiation and depression learning windows are set by $\tau_+ = \tau_- = 10$ ms. Note that the assumptions $A_+ = A_-$ and $\tau_+ = \tau_-$ are simplifications made for this particular model and not representative of biologically realistic values. We assume here that the synaptic potentiation and depression windows are equal in size, although these values could be changed as desired in the model.

For the synaptic update to occur, there must be some indication of a causal or noncausal relationship between the presynaptic neuron firing and the postsynaptic neuron firing. In this case, if $\Delta t_{\alpha\to\beta}$ falls within a predefined time window $|\Delta t_{\alpha\to\beta}| < t_c$, the synaptic update specified in Eq. (6) will occur. When $0 < \Delta t_{\alpha\to\beta} < t_c$, the presynaptic neuron fires before the postsynaptic neuron so that the relationship is causal and the synaptic strength of that relationship will correspondingly increase. Conversely, if $-t_c < \Delta t_{\alpha\to\beta} \leq 0$ (meaning that the postsynaptic neuron fires before or at the same time as the presynaptic neuron), the relationship between the neurons is noncausal and the synaptic strength will decrease (Panda et al. 2018). Outside of the $|\Delta t_{\alpha\to\beta}| < t_c$ window, no update will occur. Note that the t_c value should be selected so that a single firing relationship is not classified as both causal and noncausal over the same firing period; that is, t_c should be less than $T/2$, where T is the average period of of the coupled oscillators. In our model, we elect to use $t_c = 3$ms since the average period of the coupled oscillators (corresponding to $I_{stim} = 5$) is approximately 8.4ms. In simulations with static synaptic connections, for instance from Figs. 1 and 2, $g_{\alpha\to\beta} = 1$ for all α and β.

2.3 Phase reduction

Weakly perturbed limit cycle oscillators can be written in a reduced order form using phase reduction. Consider a general dynamical system of the form

$$\dot{x} = F(x) + \epsilon u(t), \tag{7}$$

where $x \in \mathbb{R}^N$ is the state, F sets the dynamics, u is an external perturbation, and $0 < \epsilon \ll 1$. Suppose that when $u = 0$, Eq. (7) has a stable T-periodic limit cycle x^γ, with $T = 2\pi/\omega$. States on the limit cycle can be mapped to a phase $\theta \in [0, 2\pi)$ which is scaled so that $\dot{\theta} = \omega$ where $\omega = 2\pi/T$. Using isochrons to extend phase to the basin of attraction of the limit cycle and changing variables to phase coordinates (see, for instance Ermentrout and Terman 2010; Monga et al. 2019), the phase dynamics

when $u(t) \neq 0$ can be represented according to

$$\dot{\theta} = \omega + \epsilon \frac{\partial \theta}{\partial x} \cdot u(t), \tag{8}$$

where the gradient is evaluated on the periodic orbit at $x^{\gamma}(\theta)$ and the dot denotes the dot product. In the context of the neural model (3), for neuron i, $F(x)$ denotes everything except for the synaptic current and $u(t)$ is comprised of only the synaptic current received by neuron i. Writing Eq. (3) in phase reduced form yields

$$\dot{\theta}_i = \omega_i - \frac{\epsilon}{N-1} \sum_{j \neq i} Z_i(\theta_i) \hat{K} g_{j \to i}(t) s_j(t) (V_i - E_{syn}), \tag{9}$$

for $i = 1, \ldots, N$ where $Z_i(\theta)$ is the gradient of the phase with respect to voltage perturbations evaluated on the limit cycle of the i^{th} neuron and $\hat{K} = \frac{K}{\epsilon C} > 0$. We explicitly assume that $\hat{K} = O(1)$ so that the overall input is an order ϵ term. The phase response curve can be calculated numerically using the adjoint equation or from data; we refer the interested reader to Monga et al. (2019) or Wilson and Moehlis (2022) for more information on phase reduction techniques pertaining to neuroscience applications.

With a phase reduced model that can accurately reflect the dynamics of the full order model, we can consider the Kuramoto order parameter to assess the level of synchronization of the overall population:

$$\zeta = \left| \frac{1}{N} \sum_{i=1}^{N} e^{i\theta_i} \right|. \tag{10}$$

When $\zeta = 1$ the system (9) is fully synchronized. Values of ζ closer to zero generally indicate less synchronization in the overall network but can also correspond to rotating block states (see for instance, Ashwin and Swift 1992). We consider the Kuramoto order parameter in Figs. 1 and 2 to be a general gauge of synchronization. Note that the phase is not directly measurable for simulations of (3); in this case, we take $\theta_i = 0$ to correspond to the moment that neuron i spikes and linearly interpolate all phases in between to compute (10).

3 Upper bounds for the critical coupling strength for a population of coupled neurons with synaptic plasticity

Consider a population of N tonically firing neurons of the form (3) with a Hebbian STDP update rule of the form (6). After phase reduction, the dynamics can be represented according to Eq. (9) as described in Sect. 2.3 with natural frequency $\omega \in [\omega_{min}, \omega_{max}]$. Define $\omega_0 = (\omega_{min} + \omega_{max})/2$. In this work, we use the notion of phase cohesion to characterize synchronization of the population. A population is phase cohesive at time t if there exists some arclength $\nu(t) \in [0, \pi)$ that contains θ_i for

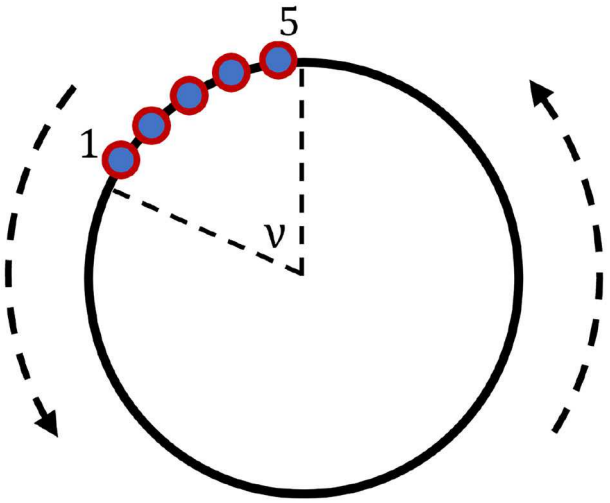

Fig. 3 Phase cohesion in a population of five neural oscillators. The phase of each oscillator is contained within the arclength ν

all $i = 1, \ldots, N$. Figure 3 provides an illustration of phase cohesion with a population $N = 5$ neural oscillators.

The goal here is to identify an upper bound on the critical coupling strength for phase cohesion. This critical coupling strength, $K_{crit}(\nu)$, is defined such that if $\hat{K} \geq K_{crit}(\nu)$, then a phase cohesive population of N neurons contained within an arclength ν will remain phase cohesive within that arclength for all forward time. To begin, let $\phi_i \equiv \theta_i - \omega_0 t$, where ϕ is a residual phase when working in a rotating reference frame (Karbowski and Ermentrout 2002). Working in this rotating reference frame, the dynamics of (9) become

$$\dot{\phi}_i = \Delta\omega_i - \epsilon \frac{\hat{K}}{N-1} \sum_{j \neq i} Z_i(\theta_i) g_{j \to i}(t) s_j(\theta_j)(V_i(\theta_i) - E_{syn}), \tag{11}$$

where $\Delta\omega_i = \omega_i - \omega_0$. Again, defining a new variable, $\psi_{i,j} = \phi_i - \phi_j$, we can write Eq. (11) in terms of the phase difference between neurons i and j.

$$\begin{aligned} \dot{\psi}_{i,j} = \omega_i - \omega_j &- \epsilon \frac{\hat{K}}{N-1} \sum_{k \neq i} \left[Z_i(\theta_i) g_{k \to i}(t) s_k(\theta_k)(V_i(\theta_i) - E_{syn}) \right] \\ &+ \epsilon \frac{\hat{K}}{N-1} \sum_{k \neq j} \left[Z_j(\theta_j) g_{k \to j}(t) s_k(\theta_k)(V_j(\theta_j) - E_{syn}) \right]. \end{aligned} \tag{12}$$

In Eq. (12), we have designated the i^{th} and j^{th} neurons to be arbitrary neurons that are presently at the leading and lagging edges of a population (neurons 1 and 5 in Fig. 3). The phase difference dynamics of any other pair of neurons contained within

this population will be bounded above by the phase difference dynamics of these edge neurons.

3.1 A limiting value of synaptic conductance when spike order is preserved

To simplify (12), we next focus on the synaptic plasticity. If two tonically-firing coupled neurons have nonidentical spike times, we define the leading neuron to be the neuron which spikes first in a given limit cycle with spike time t_{lead}, and the lagging neuron to be the neuron which spikes some time later with spike time t_{lag}, so that $0 < t_{lag} - t_{lead} < T/2$. Recall that each pair of neurons has a synaptic relationship which updates reciprocally; in our two neuron example, this means that when the relationship from the leading neuron to lagging neuron is strengthened, the relationship from the lagging neuron to the leading neuron is weakened. With this in mind, consider two neurons with phases θ_m and θ_n where neuron m, the leading neuron, always spikes before neuron n, the lagging neuron. Considering the update rule from (6), and provided ν is small enough at some initial time $t = 0$ so that the time between neuron m spiking and neuron n spiking is smaller than t_c, that is $0 < t_n - t_m < t_c$, then $g_{m\to n}$ and $g_{n\to m}$ will update reciprocally when the current lagging neuron (neuron n) fires, and $\lim_{t\to\infty}(g_{m\to n}) = 1$ while $\lim_{t\to\infty}(g_{n\to m}) = g_{min}$ regardless of initial conditions. With this in mind, for any initial condition $g_{m\to n}(0)$, where m is the leading neuron and n is the lagging neuron for all $t \geq 0$, let $t_s^{m\to n}$ be the maximum possible time required so that $|g_{m\to n}(t) - 1| \leq M$ where $M > 0$ is an order ϵ term. Correspondingly, for any initial condition $g_{n\to m}(0)$ let $t_s^{n\to m}$ be the maximum possible time required so that $|g_{n\to m}(t) - g_{min}| \leq M$. Finally, we define

$$t_s = \max(t_s^{n\to m}, t_s^{m\to n}). \tag{13}$$

Intuitively, t_s is defined so that if neuron m always spikes before neuron n on any time interval of length t_s, then $g_{m\to n}$ will be within order ϵ of its maximum value and $g_{n\to m}$ will be within order ϵ of g_{min} at the end of that time interval.

In simulations of the neural model with synaptic plasticity (3), for instance, shown in Figs. 1 and 2, and shown in detail in Fig. 4, the firing order of neurons is capable of changing over time. To accommodate this feature, we define two new variables to track potential order changes in a given time window of duration τ:

$$\rho_{i,j}(t,\tau) = \begin{cases} 1, & \text{if } \theta_j(t) = \theta_i(t) \text{ for any } t \in [t-\tau, t], \\ 0, & \text{otherwise,} \end{cases} \tag{14}$$

$$\eta_i(t,\tau) = \sum_{j\neq i} \rho_{i,j}(t,\tau). \tag{15}$$

Above, Eq. (14) tracks whether the order of θ_j and θ_i could have switched on the given time interval and (15) gives the sum of all possible ordinal switches for neuron i in that same time interval. We emphasize that the maximum value of $\rho_{i,j}(t,\tau)$ is 1, even if multiple switches occur on the given interval. An illustrative example is provided in Fig. 5 taking $\tau = 25$ for a population of $N = 25$ neurons. The leading

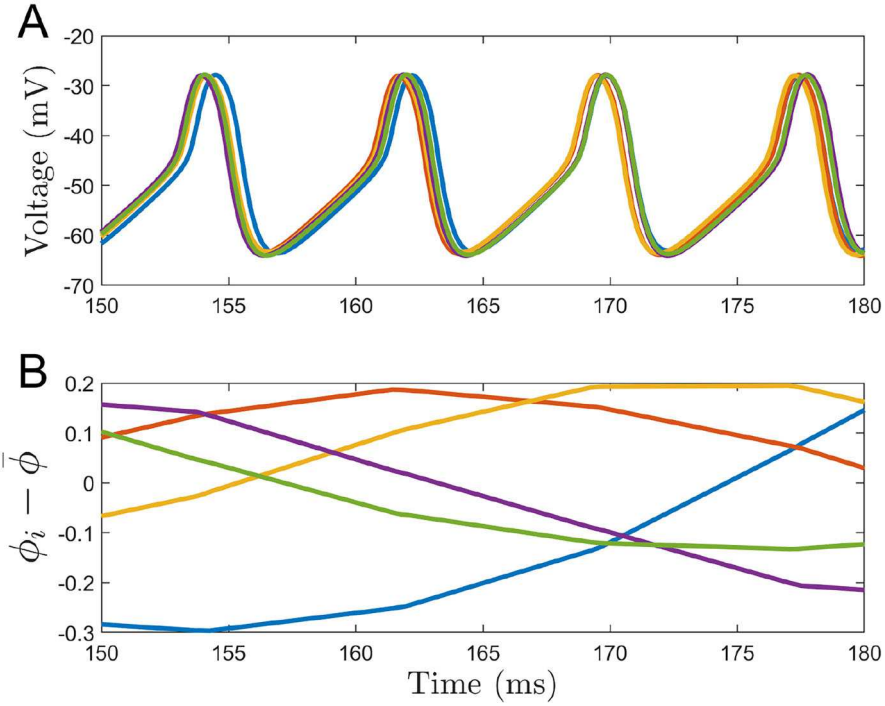

Fig. 4 A 30 ms window from a single simulation of $N = 5$ excitatory neurons with dynamics governed by (3) and the synaptic update rule in (6). Ordinal switches can be clearly seen in the full order model in panel **A** and the phase reduced model in panel **B**. In the phase reduced model, ϕ_i was computed by interpolating the phase from each neuron's respective spike times in the corresponding full order model and $\bar{\phi}(t) = \frac{1}{N}\sum_{i=1}^{N}\phi_i(t)$

(resp. lagging) edge is highlighted in panel A (resp., B). In panel A (resp., B), the black line highlights the phase of a neuron that is leading (resp., lagging) at some point in the simulation; the line is solid at all moments that the neuron is leading (resp., lagging) and dashed otherwise. In panels A and B, the phases of other neurons that change order relative to the black trace (yielding nonzero $\rho_{i,j}$) are shown in color, while all others appear in grey. All switches with the black traces in panels A and B are marked with yellow circles, and in panel A these switches are numbered 1, 2, or 3, with the number corresponding to the same numbered subplot in panel C. Panel C (resp., D) shows the value of $\rho_{i,j}(t, 25)$ associated with the change in ordering between the black trace and the trace of corresponding color from panel A (resp., B). In panel C, each $\rho_{i,j}$ is shown on its own subplot since more than one neuron switched with the neuron of interest. The first switch in panels A and B between the neuron with the black trace and the corresponding colored neuron marks the instant that $\rho_{i,j} = 1$ for that pair. Prior to this switch, $\rho_{i,j} = 0$. $\rho_{i,j}$ remains at 1 unless τ time passes without a switch. Note that per the definition from (14), $\rho_{i,j} = 1$ if neurons i and j switch one or more times on the interval $[t - \tau, t]$; multiple switches on the same interval still yield $\rho_{i,j} = 1$.

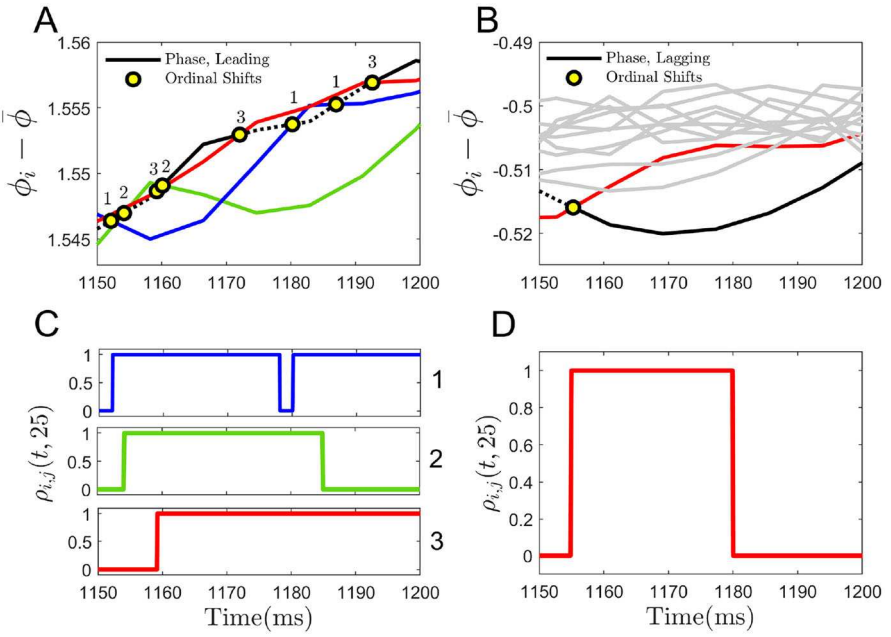

Fig. 5 Panels **A** and **B** show the phases of an example population of $N = 25$ neurons plotted with respect to the rotating reference frame. Panels **A** and **B** show the leading and the lagging edge, respectively. The black line in panel **A** (resp., B) highlights a trace associated with a single neuron that is leading (resp., lagging) at some point in the simulation; this black line is solid at the moments when this neuron is the leading (resp., lagging) neuron and dashed otherwise. For this specific neuron, all ordinal shifts are highlighted with yellow circles. In panel **A**, the yellow circles are numbered 1, 2, or 3 with the number corresponding to the identically numbered subplot in panel **C**. In panels **A** and **B**, the traces associated with neurons that do not change order with the black traces are shown in gray while those that do change order are colored. Panel **C** (resp., D) shows the value of $\rho_{i,j}(t, 25)$ associated with the change in ordering between the black trace and the trace of corresponding color from panel **A** (resp., B)

Considering the definition of t_s from Eq. (13) one can show $\rho_{i,j}(t, t_s) = 0$ implies

$$\begin{cases} g_{i\to j}(t) > 1 - M, & \text{if } \theta_i \text{ leads } \theta_j, \text{ and } \theta_\mathrm{i} - \theta_\mathrm{j} < \mathrm{t_c/T}, \\ g_{i\to j}(t) < g_{min} + M, & \text{if } \theta_j \text{ leads } \theta_i, \text{ and } \theta_\mathrm{j} - \theta_\mathrm{i} < \mathrm{t_c/T} \end{cases} \tag{16}$$

Above, recall that $M > 0$ is an $O(\epsilon)$ term and the values θ_i and θ_j are continuous functions of time and do not refer to the phase at a given spike time.

3.2 An upper bound on the critical coupling strength

To proceed, suppose that at some initial time, t_0, the phases of the neurons from (3) are contained within an arclength $\nu(t) \in [0, \pi]$ for which

$$\max_{i,j} |\theta_i(t_0) - \theta_j(t_0)| \leq \nu. \tag{17}$$

Phase cohesion is maintained so long as (17) holds for all forward time. As a reminder, for synaptic plasticity to modulate the synaptic weights in the model, the neurons need to have a causal or noncausal relationship (firing within t_c of one another). If the arclength, ν, is small enough, then there will always be a causal or anticausal relationship. Therefore, this derivation will focus on determining what coupling strength, K_{crit}, is required to ensure $\max_{i,j} |\theta_i(t) - \theta_j(t)| \leq \nu$ for all $t > t_0$.

To begin, consider any two oscillators with phases θ_m and θ_n for which $\theta_m - \theta_n = \nu$. Here, θ_m is at the leading edge of ν and θ_n is at the trailing edge. The goal here is to provide general conditions that ensure that $\dot{\theta}_m - \dot{\theta}_n \leq 0$, thereby ensuring that the phase differences do not increase beyond ν. Towards this goal, suppose that

$$\eta_k(t, t_s) \leq \beta, \tag{18}$$

for $k = \{m, n\}$, that is, the current leading and lagging neuron experience at most β order shifts in the time interval $[t - t_s, t]$. Note that (18) is an assumption that limits the amount of order switching between neurons on a given time interval. Combining Eqs. (18) and (16) with Eq. (12), one can write

$$\begin{aligned}\dot{\psi}_{m,n} \leq \omega_m - \omega_n &- \epsilon \frac{\hat{K}}{N-1} \sum_{k|\rho_{k,m}(t,t_s)=0} \left[g_{min} Z_m(\theta_m) s_k(\theta_k)(V_m(\theta_m) - E_{syn}) \right] \\ &- \epsilon \frac{\beta \hat{K}}{N-1} \min_{\theta,\upsilon} \left[\upsilon Z_m(\theta) s_k(\theta)(V_m(\theta) - E_{syn}) \right] \\ &+ \epsilon \frac{\hat{K}}{N-1} \sum_{k|\rho_{k,n}(t,t_s)=0} \left[Z_n(\theta_n) s_k(\theta_k)(V_n(\theta_n) - E_{syn}) \right] \\ &+ \epsilon \frac{\beta \hat{K}}{N-1} \max_{\theta,\upsilon} \left[\upsilon Z_n(\theta) s_k(\theta)(V_n(\theta) - E_{syn}) \right] + O(\epsilon^2),\end{aligned} \tag{19}$$

where $\upsilon \in [g_{min}, 1]$. The above inequality is obtained by considering the maximum value and minimum value for the influence of synaptic coupling from neurons that have switched order in the time interval considered, Eq. (19) can be rewritten as

$$\begin{aligned}\dot{\psi}_{m,n} \leq \dot{\mu}_{m,n} = \omega_m - \omega_n &- \epsilon \frac{\hat{K}}{N-1} \sum_{k|\rho_{k,m}(t,t_s)=0} \left[g_{min} Z_m(\theta_m) s_k(\theta_k)(V_m(\theta_m) - E_{syn}) \right] \\ &+ \epsilon \frac{\hat{K}}{N-1} \sum_{k|\rho_{k,n}(t,t_s)=0} \left[Z_n(\theta_n) s_k(\theta_k)(V_n(\theta_n) - E_{syn}) \right] + \epsilon \frac{\beta \hat{K}}{N-1}(C_1 + C_2) + O(\epsilon^2),\end{aligned} \tag{20}$$

where C_1 and C_2 are appropriately defined constants and $\mu_{m,n}$ provides an upper bound for $\psi_{m,n}$. Recalling that $\phi_i = \theta_i - \omega_0 t$, one can rewrite Eq. (20) as

$$\dot{\mu}_{m,n} = \omega_m - \omega_n - \epsilon \frac{\hat{K}}{N-1} \sum_{k|\rho_{k,m}(t,t_s)=0} \left[g_{min} Z_m(\phi_m + \omega_0 t) s_k(\phi_k + \omega_0 t)(V_m(\phi_m + \omega_0 t) - E_{syn}) \right]$$
$$+ \epsilon \frac{\hat{K}}{N-1} \sum_{k|\rho_{k,n}(t,t_s)=0} \left[Z_n(\phi_n + \omega_0 t) s_k(\phi_k + \omega_0 t)(V_n(\phi_n + \omega_0 t) - E_{syn}) \right]$$
$$+ \epsilon \frac{\beta \hat{K}}{N-1}(C_1 + C_2) + O(\epsilon^2). \tag{21}$$

Equation (21) is T_0-periodic, where $T_0 = 2\pi/\omega_0$ so that provided $\omega_m - \omega_n = O(\epsilon)$, its dynamics can be well-approximated using averaging theory (Sanders et al. 2007)

$$\dot{\mu}_{m,n} = \frac{1}{T_0} \int_0^{T_0} \Bigg(\omega_m - \omega_n + \epsilon \frac{\beta \hat{K}}{N-1}(C_1 + C_2)$$
$$- \epsilon \frac{\hat{K}}{N-1} \sum_{k|\rho_{k,m}(t,t_s)=0} \left[g_{min} Z_m(\phi_m + \omega_0 t) s_k(\phi_k + \omega_0 t)(V_m(\phi_m + \omega_0 t) - E_{syn}) \right]$$
$$+ \epsilon \frac{\hat{K}}{N-1} \sum_{k|\rho_{k,n}(t,t_s)=0} \left[Z_n(\phi_n + \omega_0 t) s_k(\phi_k + \omega_0 t)(V_n(\phi_n + \omega_0 t) - E_{syn}) \right] + O(\epsilon^2) \Bigg) dt. \tag{22}$$

Noting that the integral in Eq. (22) is evaluated over a single period, it can be rewritten in terms of the phase differences, i.e.,

$$\dot{\mu}_{m,n} = \omega_m - \omega_n + \epsilon \frac{\beta \hat{K}}{N-1}(C_1 + C_2)$$
$$- \sum_{k|\rho_{k,m}(t,t_s)=0} \left[\frac{\epsilon \hat{K}}{N-1} g_{min} \Gamma_{m,k}(\phi_m - \phi_k) \right] + \sum_{k|\rho_{k,n}(t,t_s)=0} \left[\frac{\epsilon \hat{K}}{N-1} \Gamma_{n,k}(\phi_n - \phi_k) \right], \tag{23}$$

where

$$\Gamma_{i,j}(\phi) = \frac{1}{T_0} \int_0^{T_0} Z_i(\omega_0 t) s_j(\phi + \omega_0 t)(V_i(\omega_0 t) - E_{syn}) dt. \tag{24}$$

Allowing for heterogeneity in the population of neurons, Eq. (23) can be upper bounded by

$$\dot{\mu}_{m,n} \leq \omega_m - \omega_n + \epsilon \frac{\beta \hat{K}}{N-1}(C_1 + C_2) - \sum_{k|\rho_{k,m}(t,t_s)=0} \frac{\epsilon \hat{K}}{N-1} g_{min} \Gamma_{min}(\phi_m - \phi_k)$$
$$+ \sum_{k|\rho_{k,n}(t,t_s)=0} \frac{\epsilon \hat{K}}{N-1} \Gamma_{max}(\phi_n - \phi_k), \tag{25}$$

where

$$\Gamma_{max}(\phi) = \max_{\substack{i=1,\ldots,N \\ j=1,\ldots,N}} \Gamma_{i,j}(\phi),$$

$$\Gamma_{min}(\phi) = \min_{\substack{i=1,\ldots,N \\ j=1,\ldots,N}} \Gamma_{i,j}(\phi). \tag{26}$$

Noting that $\phi_m - \phi_k \in [0, \nu]$ and $\phi_n - \phi_k \in [-\nu, 0]$ for any k, the right hand side of Eq. (25) can be bounded by

$$\dot{\mu}_{m,n} \leq \omega_m - \omega_n + \epsilon \frac{\beta \hat{K}}{N-1}(C_1 + C_2) - \frac{\epsilon \hat{K} g_{min}(N - \beta - 1)}{N-1} \min_{\phi \in (0,\nu)} \left(\Gamma_{min}(\phi)\right) + \frac{\epsilon \hat{K}(N - \beta - 1)}{N-1} \max_{\phi \in (-\nu,0)} \left(\Gamma_{max}(\phi)\right). \tag{27}$$

Above, $\phi = 0$ is not included in the maximization and minimization because otherwise $\rho_{m,k}$ and $\rho_{n,k}$ would equal 1. Considering Eq. (27), $\dot{\mu}_{m,n} \leq 0$, and hence cannot increase, provided

$$\hat{K} \geq \frac{(N-1)(\Delta\omega_{max})}{\epsilon\left[(N - \beta - 1)\left(g_{min} \min_{\phi \in (0,\nu)} (\Gamma_{min}(\phi)) - \max_{\phi \in (-\nu,0)} (\Gamma_{max}(\phi))\right) - \beta(C_1 + C_2)\right]}, \tag{28}$$

where $\Delta\omega_{max} = \max_{i,j}(\omega_i - \omega_j)$ for any possible value of i and j. Recalling that $\psi_{m,n} \leq \mu_{m,n}$, if Eq. (28) is satisfied, the phase difference between neurons m and n cannot increase. By definition, this provides an upper bound on the coupling strength to retain phase cohesion in the overall network of neurons. Recalling that $\hat{K} = \frac{K}{\epsilon C}$,

$$K_{crit}(\beta, \nu) \leq \frac{C(N-1)(\Delta\omega_{max})}{\left[(N - \beta - 1)\left(g_{min} \min_{\phi \in (0,\nu)} (\Gamma_{min}(\phi)) - \max_{\phi \in (-\nu,0)} (\Gamma_{max}(\phi))\right) - \beta(C_1 + C_2)\right]} \tag{29}$$

is an upper bound on the critical coupling strength, K, required to maintain phase cohesion. The actual critical coupling strength is guaranteed to be less than this estimated value. Notice that the bound (29) is a function of β. In the limit that the effect from order switching is negligible, $\beta = 0$ will provide an accurate estimate for the upper bound. The individual terms that comprise (29) give insight about when phase cohesion is possible. For instance, the right hand side of (29) grows with the dispersion in frequencies $\Delta\omega_{max}$ indicating that larger coupling strengths will be required when the difference in frequencies is larger. Noting that C_1 and C_2 will generally be positive and also recalling that $\hat{K}$ must be positive, $g_{min} \min_{\phi \in (0,\nu)}(\Gamma_{min}(\phi)) - \max_{\phi \in (-\nu,0)}(\Gamma_{max}(\phi)) > 0$ must be true for any upper bound on K to exist. Assuming $g_{min} \approx 0$, this would require $\Gamma_{max}(\phi) < 0$. As β increases, i.e., as the reordering of the neurons becomes faster relative to the time scales associated with the plastic synaptic conductances, the contribution from constants C_1 and C_2 increases, thereby increasing the upper bound on $\hat{K}$.

3.3 Comparison with upper bounds using static synaptic strengths

The result (29) provides an upper bound for the critical coupling strength where the synaptic weights are governed by the Hebbian STDP rule from Eq. (6). Previous work (Wilson et al. 2018) considered upper bounds for coupled inhibitory neural populations when the coupling strength is static. Excitatory neurons were not considered in Wilson et al. (2018) as phase cohesion is not possible with static synaptic coupling. Using a simplified form of the synaptic conductance

$$I_{syn}^{j\to i} = K s_j(t)(V_i - E_{syn}), \tag{30}$$

where $K > 0$ is a constant synaptic conductance and the remaining terms are defined identically to those from Eq. (2), the analysis from Wilson et al. (2018) determined the following upper bound for the critical coupling strength:

$$K_{crit}(\nu) \leq \frac{C\Delta\omega_{max}}{\min\limits_{\phi\in[0,\nu]}\left(\Gamma_{min}(\phi) - \Gamma_{max}(\phi-\nu)\right)}. \tag{31}$$

In Eq. (31), the contribution from $\Gamma_{min}(\phi)$ is weighted equally to the contribution from $\Gamma_{max}(\phi-\nu)$. As a consequence, particularly when the effect of heterogeneity is negligible, the slope of $\Gamma_{min}(\phi)$ and $\Gamma_{max}(\phi)$ is important in determining the upper bound on $\hat{K}$. Equation (31) provided a viable solution in Wilson et al. (2018) for populations of inhibitory neurons but yields an impossible solution for populations of excitatory neurons as the right hand side is negative. This is consistent with the results shown in Figs. 1 and 2 when the coupling strength is static. As a reminder, Γ_{max} and Γ_{min} are defined the same way that they were defined in Eq. (26), and so the solution presented here is dependent on our specific model parameters.

Compared to the upper bound with Hebbian plasticity (29), and considering that g_{min} is generally very close to zero, only $\Gamma_{max}(\phi)$ contributes to determining the upper bound on the critical coupling strength, which again would require $\Gamma_{max}(\phi) < 0$. This property does not hold for heterogeneous populations of inhibitory neurons. It does hold, however, for heterogeneous populations of excitatory neurons. Additionally, the ordering of the neurons within the network has a significant influence on the upper bound from (29) but has no bearing on the estimate from (31).

Figure 6 provides a visual comparison of the upper bound on K_{crit} calculated using Eqs. (31) and (29), that is with and without the inclusion of synaptic plasticity, for a population of excitatory neurons. Panels A and B show the denominator terms from Eqs. (29) and (31), respectively, while panels C and D show the corresponding values of max K_{crit}. Panel E shows the coupling functions, Γ_{max} and Γ_{min}, used in these calculations. Here $\beta = 0$ is assumed when considering the bound for the population with STDP. We emphasize that without synaptic plasticity, the right hand side of (31) is negative, indicating that no positive value of K can be chosen in order to yield phase cohesion. The results from Fig. 6 are consistent with those from Fig. 2, where the population remains phase cohesive if synaptic plasticity is considered but loses phase cohesion when there is no synaptic plasticity. Note that although we consider

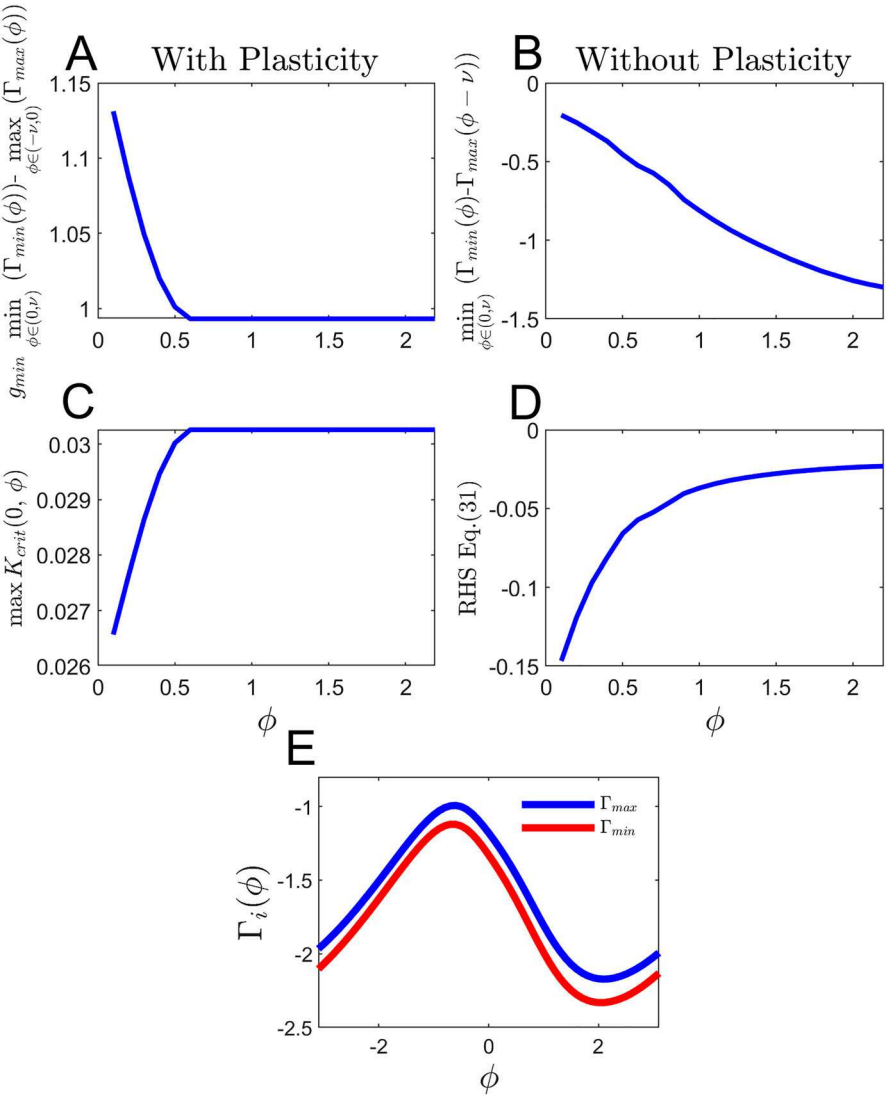

Fig. 6 Panels **A** and **B** give a visual representation of the denominator of (29) taking $\beta = 0$ and (31), respectively. Panel **C** provides the corresponding max K_{crit} for populations of excitatory neurons with plastic synaptic coupling calculated in (29). Panel **D** gives the right hand side of Eq. (31); because this value is negative, no positive value of K will result in a phase cohesive population when STDP is not considered. Panel **E** provides plots of Γ_{min} and Γ_{max} for reference

$\beta = 0$ here, this is to get an initial sense of how well this bound works for small values of β. Nonzero values of β will be considered in Sect. 4.

3.4 The critical coupling strength for inhibitory neurons

This paper has focused on the implications of STDP on the retention of phase cohesion in a population of heterogeneous excitatory neurons. However, our results would be incomplete if we did not include some of our studies on populations of inhibitory neurons. Reference (Wilson et al. 2018) found the critical coupling strength required for phase cohesion in populations of heterogeneous inhibitory neurons with static synaptic coupling. To demonstrate why inhibitory populations could not be included in this paper, we present Fig. 7. Here we have considered a population of neurons with $I_{stim} \in [4.92, 5.08]$. Note that in panels B and D, the denominator shown in Panel B is positive and the critical coupling strength is therefore positive for $\phi \in [0.2, 0.6]$, indicating that within this region, phase cohesion among these heterogeneous oscillators with inhibitory synaptic coupling is possible. Adding synaptic plasticity, however, removes the possibility of phase cohesion, as can be verified in panels A and C, which are consistently negative for all values of ϕ. Again panel E shows the coupling functions, Γ_{max} and Γ_{min}, used in these calculations.

4 Numerical results

For validation of the bound obtained in Sect. 3.2, we consider a population of N coupled excitatory neurons from Eq. (3). For these simulations $I_{stim,i} \in [4.84, 5.16]$ with specific values taken from the distributions described below. To numerically determine the actual critical coupling strength, we choose a synaptic conductance, K, (i.e., the coupling strength) larger than the critical value and slowly decrease until phase cohesion is lost. Here, we consider a population to be phase cohesive if the phases of all neurons remain within an arclength of size $\nu = 2.3$ radians.

Results are shown in Fig. 8. In each panel of Fig. 8, the upper bound on the critical coupling strength is computed according to Eq. (29), taking $\beta = 0$ and using the maximum value over all values of ϕ. This bound is shown with a dashed line for reference. In panel A, we consider populations of N = 5, 10, 15, 20, 25, and 30 excitatory neurons with baseline currents that are evenly spread between the upper and lower bounds. For each trial, the actual critical coupling strength is approximately 35 percent below the predicted critical coupling strength value. In panel B, we consider populations of neurons with two neurons having the minimum and maximum values for the baseline current and we draw the remaining baseline currents from a uniform distribution. We again consider population sizes of N = 5, 10, 15, 20, 25, and 30 excitatory neurons. For each population size considered, we numerically compute the critical coupling strength for 30 trials. Due to the randomness in each population, there is some spread in the critical coupling strengths obtained. Panel B shows the maximum, minimum, and mean of each group of 30 trials. We also consider even numbered populations of excitatory neurons where $N/2$ neurons have the smallest possible baseline current and the remaining $N/2$ neurons have the largest possible baseline current. The results for these trials are shown in panel C of Fig. 8. Particularly for these simulations, it is expected that there will be more order switching between the neurons on the boundary because the unperturbed natural frequencies are clustered

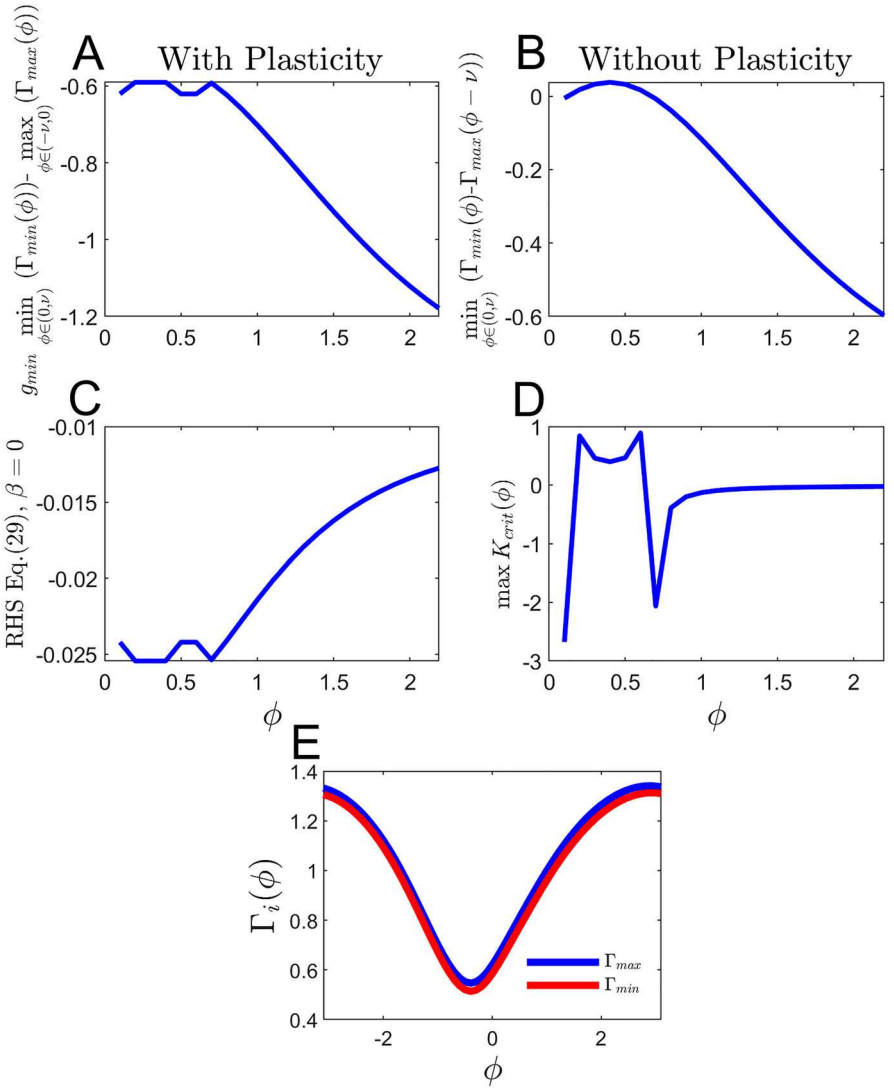

Fig. 7 Panels **A** and **B** give a visual representation of the denominator of (29) taking $\beta = 0$ and (31), respectively, for populations of inhibitory neurons with $I_{stim} \in [4.92, 5.08]$. Panel **C** provides the corresponding right hand side of Eq. (29), given $\beta = 0$ for these same populations of inhibitory neurons with plastic synaptic coupling. Since this value is negative, no positive value of K will result in a phase cohesive population when the synaptic coupling is subject to this specific form of Hebbian STDP. Panel **D** gives the upper bound on the critical coupling strength, max K_{crit}, for populations of inhibitory neurons with static synaptic coupling, which is positive in the region $\phi \in [0.2, 0.6]$. Panel **E** provides plots of Γ_{min} and Γ_{max} for reference

at the maximum and minimum values. For this reason, these simulations ultimately require a larger coupling strength to retain phase cohesion with some trials having a critical coupling strength above the value predicted from Eq. (29) for $\beta = 0$.

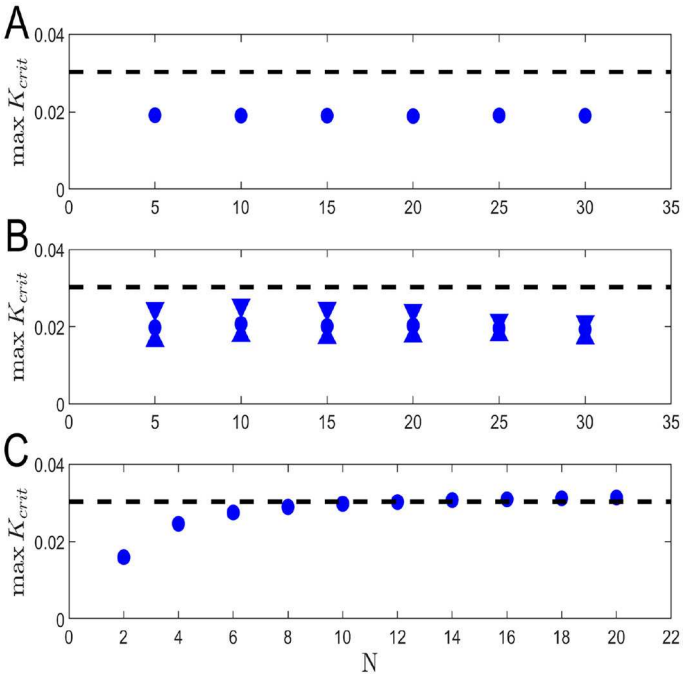

Fig. 8 In each panel, the dashed black line represents the upper bound on the critical coupling strength computed according to Eq. (29), taking $\beta = 0$ (i.e., assuming no switching between neurons on the boundary) and taking the maximum over all values of ϕ. In panel **A**, the true critical coupling strength for populations of different sizes with baseline currents spread evenly between the maximum and minimum values are shown with dots. Panel **B** is similar, except with the baseline currents drawn from a uniform distribution. Here the triangles and circles represent the minimum, average, and maximum value of the numerically computed critical coupling strength obtained from 30 total trials for each population size. In panel **C**, half of the neurons have the maximum value of baseline current and the other half have the minimum baseline current

Figure 9 is included to more carefully investigate the influence of order switching among the neurons in a population. Here we consider simulations with baseline currents taken identically to those considered in Fig. 8 and plot the corresponding η value over time for one of these simulations. Note that in each simulation, K is taken to be close to the critical value for phase cohesion. Panel A shows η calculated according to (15) for the leading and lagging neurons from a population of $N = 25$ neurons with evenly distributed natural frequencies, as was done in panel A of Fig. 8. In panel B of Fig. 9, we show the η value for a single simulation of $N = 25$ neurons where the baseline currents are drawn from a uniform distribution, as was done in panel B of Fig. 8. In panel C of Fig. 9, we finally present the η value for a simulation of N = 24 neurons with half of the natural frequencies clustered at the lower bound and half at the upper bound as was done in panel C of Fig. 8. For these trials, to ensure that our leading and lagging edge neurons were contained within and near the limits of the arclength ν, we set $K = 0.025$ in panels A and B and $K = 0.035$ in panel C. The fact that the true critical coupling strength in panel C of Fig. 8 exceeds the predicted critical

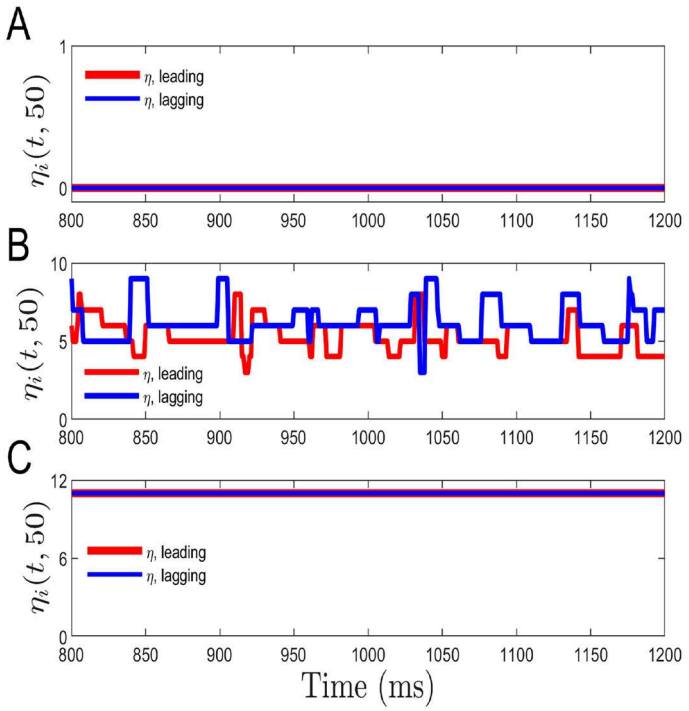

Fig. 9 In each panel, the value $\eta_i(t, 50)$ is calculated over time for a single simulation of $N = 25$ neurons in panels **A** and **B** and $N = 24$ neurons in panel **C**. For these trials the coupling strength is near the actual critical coupling strength. In panel **A**, the natural frequencies are evenly distributed as is done in panel A of Fig. 8. In panel B, the natural frequencies are taken from a uniform distribution as was done in the trials from panel **B** of Fig. 8. In panel **C**, half of the neurons have natural frequencies of ω_{max} and half of the neurons have natural frequencies of ω_{min}, as was done in the trials from panel C of Fig. 8

coupling strength is consistent with the fact that in panel C of Fig. 9, order switching is nonnegligible. Note that η is shown in these plots for the *current* leading or lagging neuron at time, t. Large jumps in η, such as those in panel B, often occur when a new neuron takes over as the leading or lagging neuron in a population. As such, when a switch occurs at the leading or lagging edge, the value of η can increase/decrease by several natural numbers in a single time step.

5 Discussion and conclusion

The presence or absence of spike timing dependent plasticity (STDP) can qualitatively alter the collective behavior of a synaptically coupled population of neurons. In this work, we derive an upper bound for the critical coupling strength required for maintaining phase cohesion in a population of conductance based, synaptically coupled neurons subject to Hebbian STDP. This work can be viewed as an extension of results from Wilson et al. (2018) (which assumed static coupling strengths between

oscillators with inhibitory connections). In addition to providing a reasonably tight upper bound on the critical coupling strength required to retain phase cohesion in populations of excitatory neurons, the results also explain the qualitative differences in the aggregate behavior in Figs. 1 and 2, where the populations are simulated with and without synaptic plasticity. When the influence of coupling felt by the leading neurons is diminished over time (as is the case here) the stability of the phase cohesive state can change depending on whether the coupling is excitatory or inhibitory.

In contrast to results that do not consider STDP, the critical coupling strength depends on the ordering of neurons. In particular, changes to the ordering of the neurons on the edge of the arclength will degrade the synchronizing influence of synaptic coupling, ultimately requiring a stronger coupling strength to retain phase cohesion. This effect is reflected in the results from Figs. 8 and 9. Individual neurons from larger populations with evenly spaced natural frequencies switch spike order less often and consequently require smaller coupling strengths to retain phase cohesion. Individual neurons from larger populations with natural frequencies clustered at the maximum and minimum values switch spike order more and hence require larger coupling strengths to retain phase cohesion. As emphasized in Figs. 8 and 9, even when the overall population remains phase cohesive, there are still a small number of order shifts between neurons in the overall population.

There are a number of limitations and possible extensions of the present work. Here, we are only concerned with the stability of the phase cohesive state but are not able to make any deductions about its basin of attraction or make inferences about spontaneous synchronization that may emerge in a coupled population of oscillators. We are also unable to make any direct inferences about frequency synchronization, although this phenomenon was not observed in any of the examples considered. Additionally, we do not directly consider the influence of noise in the population which would certainly be a factor in a more realistic population of neural oscillators. Furthermore, the phase-based reduction techniques used here are only valid in the weakly perturbed limit and it may be necessary to incorporate alternative phase-based reduction strategies that can accommodate larger magnitude inputs in more realistic models. We elected to use soft bound Hebbian STDP in our model, which does not allow for unrestricted growth or decay of a given synaptic connection, bounding the synaptic strength so that $g_{i\to j} \in [g_{min}, 1]$ and $|\Delta g_{i\to j}|$ decreases as the synaptic strength approaches a boundary. However, there exist qualitative differences when hard bounds are implemented instead, where the update to the synaptic connection is linearly additive and no longer a function of the current synaptic weight. Some of these qualitative differences, such as those mentioned in Van Rossum et al. (2012) and Gütig et al. (2003), could affect these results. It would be of interest to conduct further analysis on how hard bounds would alter the findings presented here. Finally, the analysis considered in this work is only valid for tonically firing neurons and it would be of interest to investigate possible extensions for bursting neurons or for neurons without a well-defined firing rate.

Data availability Data sharing not applicable to this article as no datasets were generated or analysed during the current study.

Declarations

Conflict of interest This material is based upon the work supported by the National Science Foundation (NSF) under Grant No. CMMI-1933583.

References

Ashwin P, Swift JW (1992) The dynamics of *n* weakly coupled identical oscillators. J Nonlinear Sci 2:69–108

Brown E, Holmes P, Moehlis J (2003) Globally coupled oscillator networks. In: Kaplan E, Marsden J, Sreenivasan KR (eds) Nonlinear science: a celebratory volume in honor of Larry Sirovich. Springer, Berlin, pp 183–215

Chialvo DR (2010) Emergent complex neural dynamics. Nat Phys 6(10):744–750

Dayan P, Abbott LF (2001) Theoretical neuroscience. MIT Press, Cambridge

Ermentrout B (1996) Type I membranes, phase resetting curves, and synchrony. Neural Comput 8:979–1001

Ermentrout GB, Terman DH (2010) Mathematical foundations of neuroscience. Springer, Berlin

Golombek DA, Rosenstein RE (2010) Physiology of circadian entrainment. Physiol Rev 90(3):1063–1102

Gütig R, Aharonov R, Rotter S, Sompolinsky H (2003) Learning input correlations through nonlinear temporally asymmetric Hebbian plasticity. J Neurosci 23(9):3697–3714

Hansel D, Mato G, Meunier C (1995) Synchrony in excitatory neural networks. Neural Comput 7:307–337

Hipp JF, Engeland AK, Siegel M (2011) Oscillatory synchronization in large-scale cortical networks predicts perception. Neuron 69(2):387–396

Ho VM, Lee J, Martin KC (2011) The cell biology of synaptic plasticity. Science (American Association for the Advancement of Science) 334(6056):623–628

Holt AB, Wilson D, Shinn M, Moehlis J, Netoff TI (2016) Phasic burst stimulation: a closed-loop approach to tuning deep brain stimulation parameters for Parkinson's disease. PLOS Comput Biol 13:e1005011

Hoppensteadt FC, Izhikevich EM (1997) Weakly connected neural networks. Springer, New York

Iakymchuk T, Rosado-Muñoz A, Guerrero-Martínez JF, Bataller-Mompeán M, Francés-Víllora JV (2015) Simplified spiking neural network architecture and STDP learning algorithm applied to image classification. EURASIP J Image Video Process 2015(1):1–11

Karbowski J, Ermentrout GB (2002) Synchrony arising from a balanced synaptic plasticity in a network of heterogeneous neural oscillators. Phys Rev E 65(3):031902

Kennedy MB (2013) Synaptic signaling in learning and memory. Cold Spring Harb Perspect Biol 8(2):a016824–a016824

Khoshkhou M, Montakhab A (2019) Spike-timing-dependent plasticity with axonal delay tunes networks of Izhikevich neurons to the edge of synchronization transition with scale-free avalanches. Front Syst Neurosci 13:73

Levina A, Herrmann JM, Geisel T (2007) Dynamical synapses causing self-organized criticality in neural networks. Nat Phys 3(12):857–860

Levy N, Horn D, Meilijson I, Ruppin E (2001) Distributed synchrony in a cell assembly of spiking neurons. Neural Netw 14(6–7):815–824

Maistrenko YL, Lysyansky B, Hauptmann C, Burylko O, Tass PA (2007) Multistability in the Kuramoto model with synaptic plasticity. Phys Rev E 75(6):066207

Manna DL, Vicente-Sola A, Kirkland P, Bihl TJ, Di Caterina G (2022) Simple and complex spiking neurons: perspectives and analysis in a simple STDP scenario. Neuromorphic Comput Eng 2(4):044009

Monga B, Wilson D, Matchen T, Moehlis J (2019) Phase reduction and phase-based optimal control for biological systems: a tutorial. Biol Cybern 113(1):11–46

Nowotny T, Zhigulin VP, Selverston AI, Abarbanel HDI, Rabinovich MI (2003) Enhancement of synchronization in a hybrid neural circuit by spike-timing dependent plasticity. J Neurosci 23(30):9776–9785

Ozkan ZA, Bose A, Nadim F (2014) Effects of synaptic plasticity on phase and period locking in a network of two oscillatory neurons. J Math Neurosci 4:8

Panda P, Allred JM, Ramanathan S, Roy K (2018) ASP: Learning to forget with adaptive synaptic plasticity in spiking neural networks. IEEE J Emerg Sel Top Circuits Syst 8(1):51–64
Pogosyan A, Yoshida F, Chen CC, Martinez-Torres I, Foltynie T, Limousin P, Zrinzo L, Hariz MI, Brown P (2010) Parkinsonian impairment correlates with spatially extensive subthalamic oscillatory synchronization. Neuroscience 171(1):245–257
Pyragas K, Fedaravičius AP, Pyragienė T, Tass PA (2018) Optimal waveform for entrainment of a spiking neuron with minimum stimulating charge. Phys Rev E 98(4):042216
Reppert SM, Weaver DR (2002) Coordination of circadian timing in mammals. Nature 418(6901):935
Rubin JE, Terman D (2004) High frequency stimulation of the subthalamic nucleus eliminates pathological thalamic rhythmicity in a computational model. J Comput Neurosci 16(3):211–235
Sanders JA, Verhulst F, Murdock J (2007) Averaging methods in nonlinear dynamical systems, 2nd edn. Springer, New York
Senkowski D, Schneider TR, Foxe JJ, Engel AK (2008) Crossmodal binding through neural coherence: implications for multisensory processing. Trends Neurosci 31(8):401–409
Toth K, Wilson D (2022) Control of coupled neural oscillations using near-periodic inputs. Chaos Interdiscip J Nonlinear Sci 32(3):033130
Van Rossum MCW, Shippi M, Barrett AB (2012) Soft-bound synaptic plasticity increases storage capacity. PLoS Comput Biol 8(12):e1002836
Van Vreeswijk C, Abbott LF, Ermentrout GB (1994) When inhibition not excitation synchronizes neural firing. J Comput Neurosci 1(4):313–321
Wichmann T, DeLong MR, Guridi J, Obeso JA (2011) Milestones in research on the pathophysiology of Parkinson's disease. Mov Disord 26(6):1032–1041
Wilson D (2020) Optimal open-loop desynchronization of neural oscillator populations. J Math Biol 81(1):25–64
Wilson D, Faramarzi S, Moehlis J, Tinsley MR, Showalter K (2018) Synchronization of heterogenous oscillator populations in response to weak and strong coupling. Chaos Interdiscip J Nonlinear Sci 28(12):123114
Wilson D, Moehlis J (2022) Recent advances in the analysis and control of large populations of neural oscillators. Annu Rev Control 54:327–351